


RESEARCH ARTICLE

Peripheral macrophages drive CNS disease in the *Ndufs4*(-/-) model of Leigh syndrome

Allison R. Hanaford¹ | Asheema Khanna² | Vivian Truong¹ | Katerina James¹ |
 Yihan Chen¹ | Michael Mulholland¹ | Bernhard Kayser¹ | Ryan W. Liao¹ |
 Margaret Sedensky^{1,3} | Phil Morgan^{1,3} | Nathan Andrew Baertsch^{1,4} |
 Vandana Kalia^{2,4} | Surojit Sarkar^{2,4} | Simon C. Johnson^{1,3,5,6,7} 

¹Center for Integrative Brain Research, Seattle Children's Research Institute, Seattle, Washington, USA

²Ben Towne Center for Childhood Cancer Research, Seattle Children's Research Institute, Seattle, Washington, USA

³Department of Anesthesiology and Pain Medicine, University of Washington, Seattle, Washington, USA

⁴Department of Pediatrics, University of Washington School of Medicine, Seattle, Washington, USA

⁵Department of Laboratory Medicine and Pathology, University of Washington, Seattle, Washington, USA

⁶Department of Neurology, University of Washington, Seattle, Washington, USA

⁷Department of Applied Sciences, Translational Bioscience, Northumbria University, Newcastle Upon Tyne, UK

Correspondence

Simon C. Johnson, Faculty of Health and Life Sciences, Northumbria University, A521A Ellison Building, Newcastle Upon Tyne, NE1 8ST, UK.

Email: simon.c.johnson@northumbria.ac.uk

Funding information

Mitochondrial Research Guild; National Institute for Health and Care Research, Grant/Award Numbers: R01-133865, R01NS119426

Abstract

Subacute necrotizing encephalopathy, or Leigh syndrome (LS), is the most common pediatric presentation of genetic mitochondrial disease. LS is a multi-system disorder with severe neurologic, metabolic, and musculoskeletal symptoms. The presence of progressive, symmetric, and necrotizing lesions in the brainstem are a defining feature of the disease, and the major cause of morbidity and mortality, but the mechanisms underlying their pathogenesis have been elusive. Recently, we demonstrated that high-dose pexidartinib, a CSF1R inhibitor, prevents LS CNS lesions and systemic disease in the *Ndufs4*(-/-) mouse model of LS. While the dose-response in this study implicated peripheral immune cells, the immune populations involved have not yet been elucidated. Here, we used a targeted genetic tool, deletion of the colony-stimulating Factor 1 receptor (CSF1R) macrophage super-enhancer FIRE (*Csf1r*ΔFIRE), to specifically deplete microglia and define the role of microglia in the pathogenesis of LS. Homozygosity for the *Csf1r*ΔFIRE allele ablates microglia in both control and *Ndufs4*(-/-) animals, but onset of CNS lesions and sequelae in the *Ndufs4*(-/-), including mortality, are only marginally impacted by microglia depletion. The overall development of necrotizing CNS lesions is not altered, though microglia remain absent. Finally, histologic analysis of brainstem lesions provides direct evidence of a causal role for peripheral macrophages in the characteristic CNS lesions. These data demonstrate that peripheral macrophages play a key role in the pathogenesis of disease in the *Ndufs4*(-/-) model.

KEYWORDS

CNS lesions, Leigh syndrome, microglia, mitochondrial disease, pediatric disease, subacute necrotizing encephalomyelopathy

1 | INTRODUCTION

Subacute necrotizing encephalomyelopathy, Leigh syndrome (LS), is the most common pediatric presentation of genetic mitochondrial disease [1, 2]. LS neuropathology is

Dedication: We dedicate this study to Colson Morris, Liz, and Jacob Morris, their family, and all those living with the consequences of mitochondrial disease. They continue to inspire us.

This is an open access article under the terms of the [Creative Commons Attribution-NonCommercial-NoDerivs](https://creativecommons.org/licenses/by-nc-nd/4.0/) License, which permits use and distribution in any medium, provided the original work is properly cited, the use is non-commercial and no modifications or adaptations are made.

© 2023 The Authors. *Brain Pathology* published by John Wiley & Sons Ltd on behalf of International Society of Neuropathology.

characterized by symmetric, bilateral, neurodegenerative lesions, which can appear in the basal ganglia, brainstem, and cerebellum [1, 3]. Patients are often born without evidence of disease, and symptoms typically first present in early childhood with progressive psychomotor regression and symptoms related to brainstem pathology (e.g., respiratory issues, dysphagia) [1]. LS is clinically defined and genetically heterogeneous disease, complicating diagnosis and study. To date, LS has been causally linked to more than 75 distinct genes [2]. These include genes encoded by both nuclear and mitochondrial genomes, coding for proteins involved in electron transport chain (ETC) or ETC complex assembly factors, mitochondrial transcription/translation factors, and enzymes involved in thiamine metabolism [2].

One causal gene for LS in humans is *NDUFS4*, coding for a structural/assembly component of ETC complex I. Homozygous deletion of murine *Ndufs4* results in a LS phenotype in mice, and the *Ndufs4*($-/-$) mouse is considered the premier animal model of mitochondrial disease. *Ndufs4*($-/-$) mice present with a multi-system disorder similar to human patients, which includes necrotic lesions in the brainstem, neurological and metabolic dysfunction, and early mortality [4, 5]. Neuroinflammation and lesions also develop in cerebellum. CNS lesions in the brainstem, olfactory bulb, and cerebellum of *Ndufs4*($-/-$) mice are characterized by astrogliosis and microgliosis. Advanced brainstem lesions are well demarcated, developing into densely packed IBA1(+) phagocytic cells with astrocyte accumulation (typically observed via staining with GFAP) surrounding the central lesion. The olfactory bulb and cerebellar neuroinflammation also display increased IBA1(+) cell and astrogliosis.

We have recently demonstrated that disease in the *Ndufs4*($-/-$) is causally mediated by immune cells, and that treatment with the Colony Stimulating Factor 1 Receptor (CSF1R) inhibitor pexidartinib/PLX3397 can provide potent therapeutic benefits [6]. CSF1R regulates the differentiation, function, and survival of macrophages, including microglia [7]. High-dose pexidartinib depletes both CNS and peripheral macrophages, but the effect is relatively microglia-specific when administered at low dose, and low-dose pexidartinib has been reproducibly used as an experimental tool for microglia depletion [8, 9].

Phagocytic cell accumulation in LS lesions has been interpreted as microgliosis, with no consideration of a role for peripheral cells [10, 11]. However, histologic methods and markers used in prior studies have been non-specific, including the pan-macrophage marker IBA1 and morphologic analysis [11, 12]. In our recent work, we found that low doses of pexidartinib (sufficient to deplete microglia but not peripheral macrophages) fail to substantially alter disease course, while high doses prevent disease. Moreover, staining of lesions using a TMEM119-GFP reporter revealed that a substantial fraction of IBA1(+) cells in CNS lesions do not express

this microglia-specific marker [6, 13]. Defining the roles of individual phagocytic cell populations is important for developing immune-targeting strategies into therapies, as CNS microglia and peripheral macrophages have distinct pharmacological properties and targets. In addition, defining the relative roles of peripheral and central macrophages will have significant impact on our basic understanding of the pathogenesis of this mitochondrial disease.

To determine the role of microglia in the pathobiology of LS, here we utilize a genetic model for microglia depletion, the *Csf1r* Δ FIRE mouse [14]. These animals carry deletion of an *fms*-intronic regulator element (FIRE) in the *Csf1r* gene, an element which regulates expression of *Csf1r* in microglia [14, 15]. Mice homozygous for the *Csf1r* Δ FIRE allele (here abbreviated *Csf1r*[fr/fr] with *Csf1r*[wt/fr] and *Csf1r*[wt/wt] denoting heterozygous and wild-type for this allele, respectively) lack microglia and some tissue macrophage populations, but have intact circulating macrophages [14]. Here, we report the impact of genetic depletion of microglia on disease and survival in the *Ndufs4*($-/-$) model. In addition, we directly assess the presence of microglia and peripheral macrophages in LS CNS lesions. Our findings support a model whereby peripheral macrophages are a primary causal cell type in the pathogenesis of LS CNS lesions.

2 | RESULTS

2.1 | Homozygosity for the *Csf1r* Δ FIRE allele results in depletion of microglia in control and *Ndufs4*($-/-$) mice

To confirm the impact of the *Csf1r* Δ FIRE allele on microglia populations in our mouse model, we generated an *Ndufs4*($+/-$)/*Csf1r*(wt/fr) colony (*Csf1r* Δ FIRE mice in the C57Bl/6 background generously provided by the Blurton-Jones laboratory at UC Irvine, derived from animals provided by the Pridans Laboratory at University of Edinburgh, see Section 4 for breeding and backcrossing details). Immunofluorescent staining for IBA1 in control animals for the *Ndufs4* gene confirmed the impact of the *Csf1r* Δ FIRE deletion on microglia: *Ndufs4*(control)/*Csf1r*(fr/fr) samples were devoid of IBA1 positive cells in the brain, consistent with prior reports of the impact of the *Csf1r* Δ FIRE allele (Figure 1A–G, see Section 4 for genotype details; see Figures S1–S9 for enlarged panels from Figure 1) [14]. Heterozygosity for the *Csf1r* Δ FIRE allele in *Ndufs4*(control)/*Csf1r*(wt/fr) mice did not significantly impact microglia numbers compared to *Ndufs4*(control)/*Csf1r*(wt/wt) animals (Figure 1B–G).

Despite lacking microglia, we observed that, as previously reported, *Csf1r*(fr/fr) mice have no overt phenotype with the exception of an increased incidence hydrocephalus (observed in \sim 15% *Csf1r*(fr/fr) pups, versus $<$ 1% in C57Bl/6

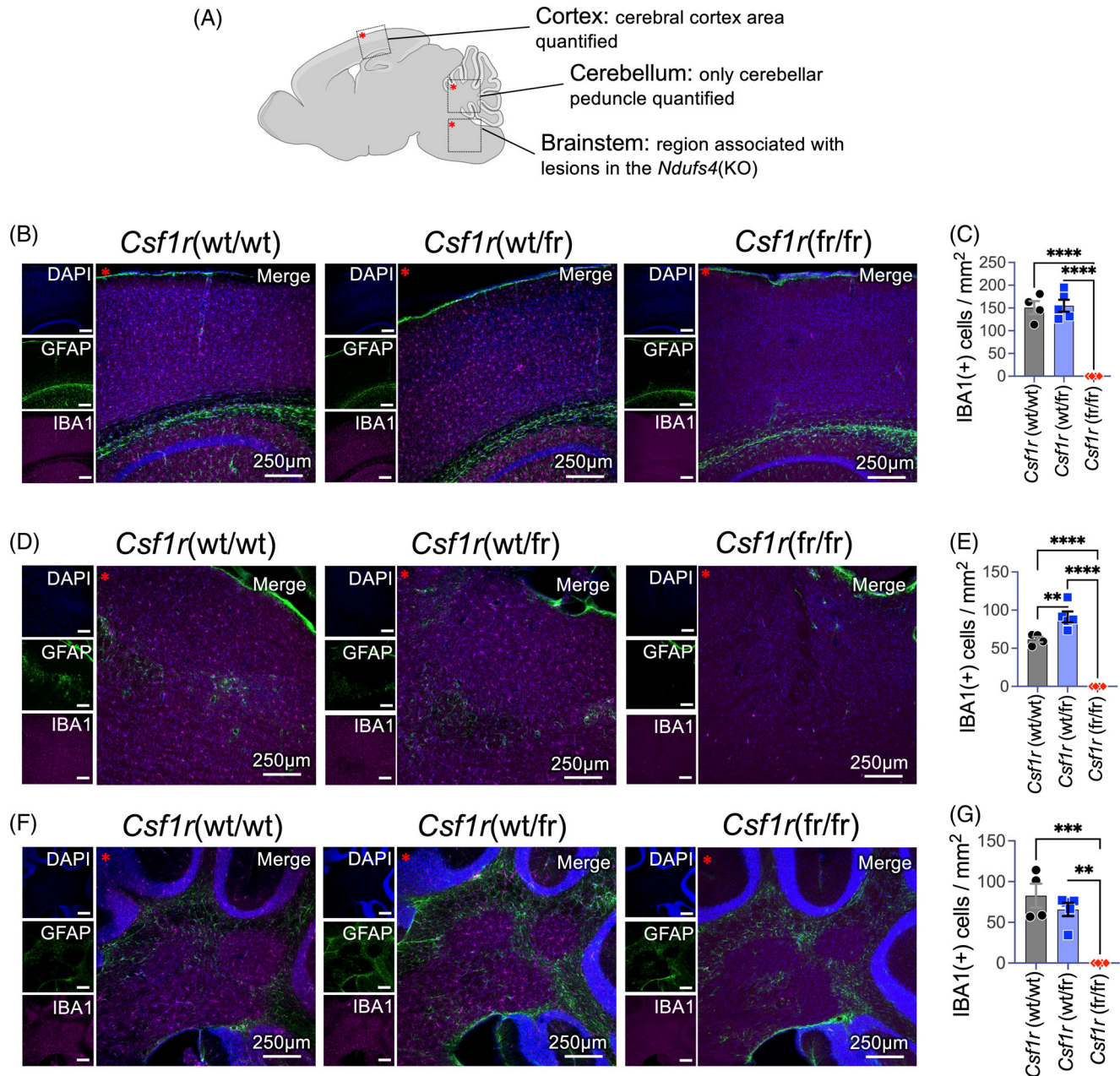


FIGURE 1 Depletion of microglia in *Csf1r*(fr/fr) mice. (A) Diagram of brain regions imaged and analyzed. In cortex, microglia numbers were only quantified in the cerebral cortex area. In cerebellum, microglia were quantified in the peduncle. In the brainstem, microglia were quantified within the brainstem region where CNS lesions develop in the *Ndufs4*(-/-) model, adjacent to the fourth ventricle and inferior to the cerebellum. Only *Ndufs4* controls are assessed in this figure (see Section 4 for genotype details, Figures 3 and 4). For all immunofluorescence panels, location of red asterisks in diagram (A) and in merged immunofluorescence images show relative orientation. (B) Representative images of cortex from *Csf1r*(wt/wt), *Csf1r*(wt/fr), and *Csf1r*(fr/fr), *Ndufs4*(control), mice. (C) Quantification of microglia numbers within the cerebral cortex. **** $p < 0.0001$ by one-way ANOVA. (D) Representative images of the LS CNS lesion associated region of the brainstem in *Csf1r*(wt/wt), *Csf1r*(wt/fr), and *Csf1r*(fr/fr), *Ndufs4*(control), mice. (E) Quantification of microglia numbers within the lesion-associated brainstem region. **** $p < 0.0001$ by one-way ANOVA. (F) Representative images of the cerebellar peduncle in *Csf1r*(wt/wt), *Csf1r*(wt/fr), and *Csf1r*(fr/fr), *Ndufs4*(control), mice. (G) Quantification of microglia numbers within the cerebellar peduncle. *** $p = 0.003$ by one-way ANOVA. (C,E,G) Error bars are standard error of the mean. Tukey's multiple comparisons corrected p -values for pairwise comparisons. ** $p < 0.005$, *** $p < 0.0005$, **** $p < 0.00005$. $n = 4$ biological replicates per group per brain regions (see Section 4). (B–G) tissues collected from animals aged P60–65. See Figures S1–S9 for enlargements of panels in Figure 1.

per Jackson Laboratories data). These observations generally agree with prior reports of a hydrocephalus rate of ~5% in *Csf1r*(fr/fr) animals, and hydrocephaly in *Csf1r* null mice [16, 17]. Hydrocephalus is already increased in

many inbred mouse strains, including C57Bl/6, and as standard practice pups with hydrocephaly are euthanized regardless of genotype and not included in experiments (see Section 4).

2.2 | Neuroinflammation in microglia-depleted *Ndufs4*(*-/-*) animals

We next assessed the impact of the *Csf1r* Δ FIRE allele on neuroinflammation in *Ndufs4*(*-/-*) mice. Immunofluorescent staining of cerebellum and ventral brainstem demonstrated that while a single copy of the *Csf1r* Δ FIRE allele did not significantly impact microglia numbers, *Ndufs4*(*-/-*)/*Csf1r*(*fr/fr*) mice lack IBA1(+) cells in cortex and in brainstem areas not associated with CNS lesions in *Ndufs4*(*-/-*) mice (Figure 2; see Figures S10–S15 for enlarged panels from Figure 2).

While microglia were absent in regions not associated with lesion formation, necrotizing CNS lesions were not prevented: as in *Ndufs4*(*-/-*) mice with wild-type *Csf1r*, *Ndufs4*(*-/-*)/*Csf1r*(*fr/fr*) mice at about post-natal

day 60 (P60) presented with overt lesions in the brainstem and olfactory bulb comprised of the typical composition of IBA1(+) and GFAP(+) cells (Figure 3A–G; see Figures S16–S21 for enlarged panels from Figure 3). Critically, in brain tissue immediately adjacent to the lesions, IBA1(+) cells remain absent (Figure 3C, see area adjacent to lesion; see also Figure 2). The cerebellar peduncle also remained IBA1(+) cell free, possibly uncoupling cerebellar and brainstem lesions, at least at ~P60 (Figure 3G).

2.3 | Impact of *Csf1r* Δ FIRE allele on disease progression and survival in *Ndufs4*(*-/-*) mice

To assess the impact of microglia depletion on disease and survival in the *Ndufs4*(*-/-*) model of LS, we next

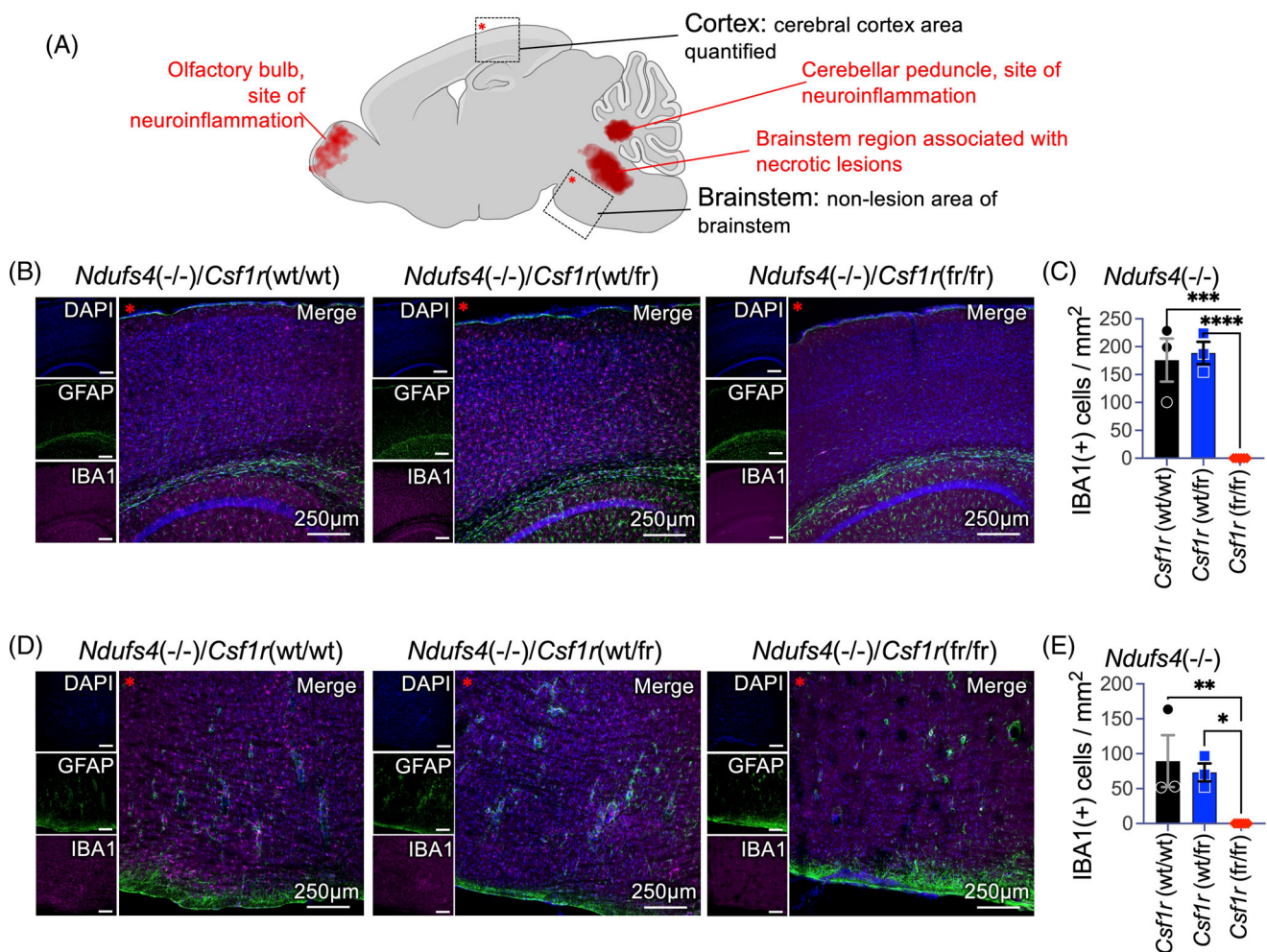


FIGURE 2 Depletion of microglia in *Ndufs4*(*-/-*)/*Csf1r*(*fr/fr*) mice. (A) Diagram of brain regions associated with neuroinflammatory lesions in the *Ndufs4*(*-/-*) model (red highlighted), and the cortex and brainstem regions imaged and analyzed in this figure. For all immunofluorescence panels, location of red asterisks in diagram (A) and in merged immunofluorescence images show relative orientation. (B) Representative images of cortex from *Ndufs4*(*-/-*)/*Csf1r*(*wt/wt*), *Ndufs4*(*-/-*)/*Csf1r*(*wt/fr*), and *Ndufs4*(*-/-*)/*Csf1r*(*fr/fr*) mice. (C) Quantification of microglia numbers within the cerebral cortex. *****p* < 0.0001 by one-way ANOVA. (D) Representative images of ventral brainstem region adjacent to areas of lesion formation in *Ndufs4*(*-/-*)/*Csf1r*(*wt/wt*), *Ndufs4*(*-/-*)/*Csf1r*(*wt/fr*), and *Ndufs4*(*-/-*)/*Csf1r*(*fr/fr*) mice. (E) Quantification of microglia numbers within the lesion-associated brainstem region. *****p* < 0.0001 by one-way ANOVA. (C,E) Error bars are standard error of the mean. Tukey's multiple comparisons corrected *p*-values for pairwise comparisons. ***p* < 0.005, ****p* < 0.0005, *****p* < 0.00005. *n* = 2–3 biological replicates per group per brain regions (see Section 4). Tissues collected from animals aged P55–66. See Figures S10–S15 for enlargements of panels in Figure 2.

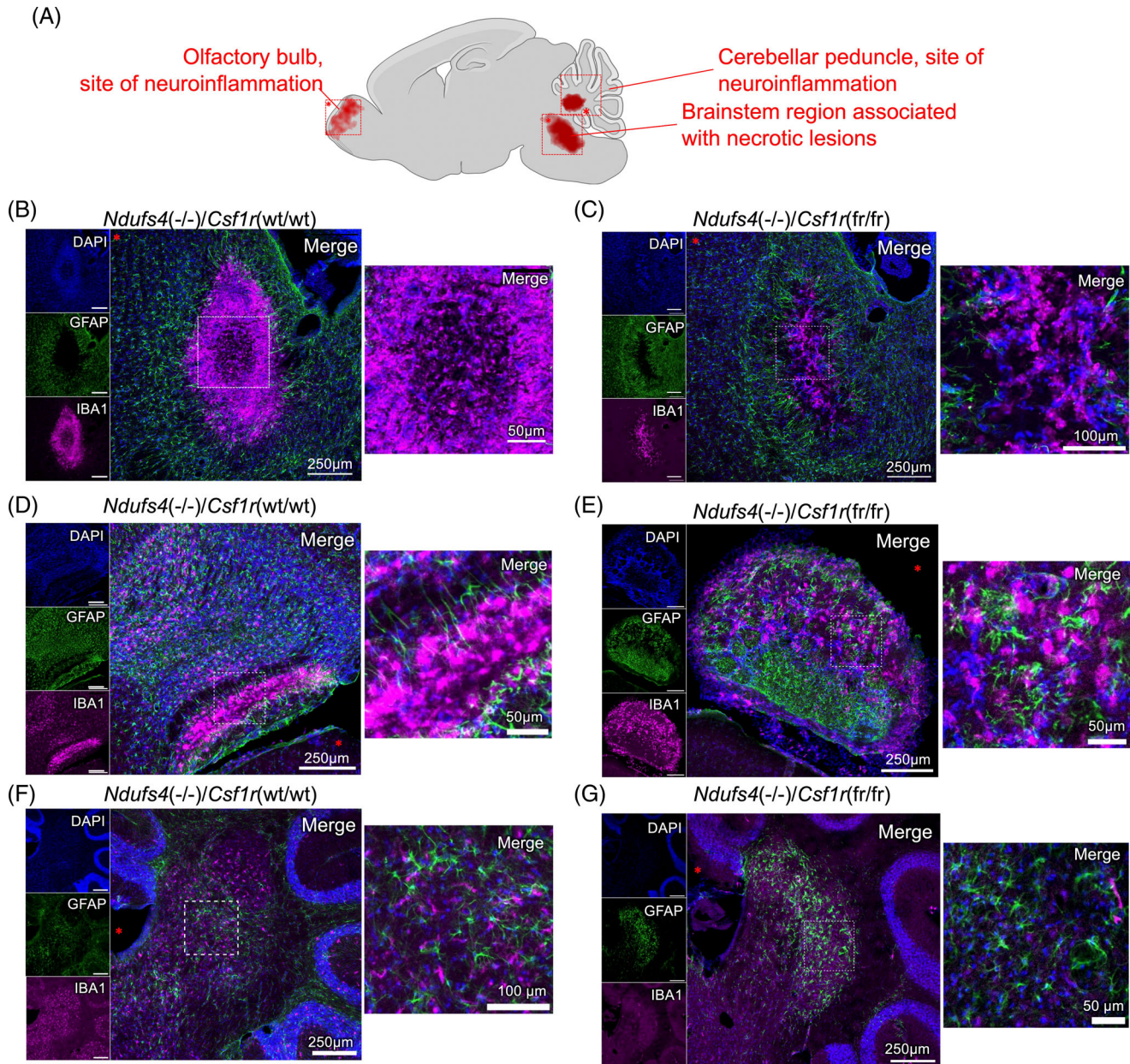


FIGURE 3 CNS lesions in *Ndufs4(-/-)/Csf1r(wt/wt)* and *Ndufs4(-/-)/Csf1r(fr/fr)* mice. (A) Diagram of brain regions associated with neuroinflammatory lesions in the *Ndufs4(-/-)* model and the regions shown in this figure. For all immunofluorescence panels, location of red asterisks in diagram (A) and in merged immunofluorescence images show relative orientation. (B,C) Brainstem CNS lesions in *Ndufs4(-/-)/Csf1r(wt/wt)* (B) and *Ndufs4(-/-)/Csf1r(fr/fr)* (C) mice. (D,E) Olfactory bulb CNS neuroinflammation in *Ndufs4(-/-)/Csf1r(wt/wt)* (D) and *Ndufs4(-/-)/Csf1r(fr/fr)* (E) mice. (F-G) Cerebellar peduncle in *Ndufs4(-/-)/Csf1r(wt/wt)* (F) and *Ndufs4(-/-)/Csf1r(fr/fr)* (G) mice. IBA1(+) cells remain absent in this LS neuroinflammation associated region in *Ndufs4(-/-)/Csf1r(fr/fr)* mice. (B-G) All images are representative of staining of at least three biological replicates. Tissues collected from animals aged P55–66. See Figures S16–S21 for enlargements of panels in Figure 3.

assess survival of *Ndufs4(-/-)* mice wild-type, heterozygous, or homozygous for the *Csf1r*ΔFIRE allele. In the *Ndufs4(-/-)* model, animals lack overt symptoms of disease until around ~P37 (see [6, 11]). Around this age, animals begin to lose weight (defined here as cachexia), display signs of forelimb clasp and ataxia, develop progressively worsening hypoglycemia, and show a progressive decline in performance on the rotarod assay for overall endurance

and neuromuscular coordination (see Section 4). Onset and progression of weight loss was not significantly delayed in either *Ndufs4(-/-)/Csf1r(wt/wt)* or *Ndufs4(-/-)/Csf1r(fr/fr)* animals compared to *Ndufs4(-/-)/Csf1r(wt/wt)* mice (Figure 4A,B). Moreover, *Ndufs4(-/-)/Csf1r(fr/fr)* showed only marginal benefits to symptoms of disease: delays in onset of ataxia and forelimb clasp were statistically significantly, but extremely modest (Figure 4C).

Median survival was modestly, but statistically significantly, increased in both *Ndufs4(-/-)/Csf1r(fr/fr)* and *Ndufs4(-/-)/Csf1r(wt/fr)* animals compared to the *Ndufs4(-/-)/Csf1r(wt/wt)* group (Figure 4F). In contrast with the benefits of CSF1R inhibition with pexidartinib, respiratory rate defects associated with brainstem lesion progression were not rescued in *Ndufs4(-/-)/Csf1r(fr/fr)* and *Ndufs4(-/-)/Csf1r(wt/fr)* mice (Figure S22). Microglia depletion did not alter the primary cause of death in *Ndufs4(-/-)* animals, which was euthanasia caused by reaching weight-loss criteria in all *Ndufs4(-/-)* cohorts, though a greater fraction of animals died before reaching the 20% weight cut-off (Figure 4G, see Section 4).

2.4 | Peripheral macrophages in CNS lesions

Given these findings, we next sought to assess the presence of microglial and peripheral macrophage markers in IBA1(+) cells present in the CNS lesions in the *Ndufs4(-/-)* model. Co-staining of brain slices using antibodies targeting IBA1 and the microglia-specific marker

P2YR12 further validated the loss of microglia in cortex (Figure 5A,B; see Figures S23–S30 for enlarged panels from Figure 5). In *Ndufs4(-/-)/Csf1r(fr/fr)* mice, brainstem lesions were found to be composed of IBA1(+)/P2YR12(-) cells, likely peripheral macrophages (Figure 5C,D). In the *Ndufs4(-/-)/Csf1r(wt/wt)*, IBA1(+) cells in the brainstem lesion show P2YR12 positivity, indicating that microglia make up the bulk of the lesions in animals not carrying the $\Delta FIRE$ allele. Overall cellularity of the lesions was reduced in *Csf1r(fr/fr)* (as determined by DAPI nuclei density and numbers in the lesion core), and the *Csf1r(wt/wt)* animals show some P2YR12 positivity, supporting the notion that microglia are present in lesions in animals with an intact *CSF1R* allele.

Similarly, co-staining with IBA1 and the peripheral (hematopoietic origin) immune cell marker CD45 revealed that IBA1(+) cells in *Ndufs4(-/-)/Csf1r(fr/fr)* mice are, indeed, peripheral in origin (Figure 5E,H). Staining of *Ndufs4(-/-)/Csf1r(wt/wt)* mice verified that microglia in cortex are CD45(-), while some CD45(+) are present and show non-microglial morphology

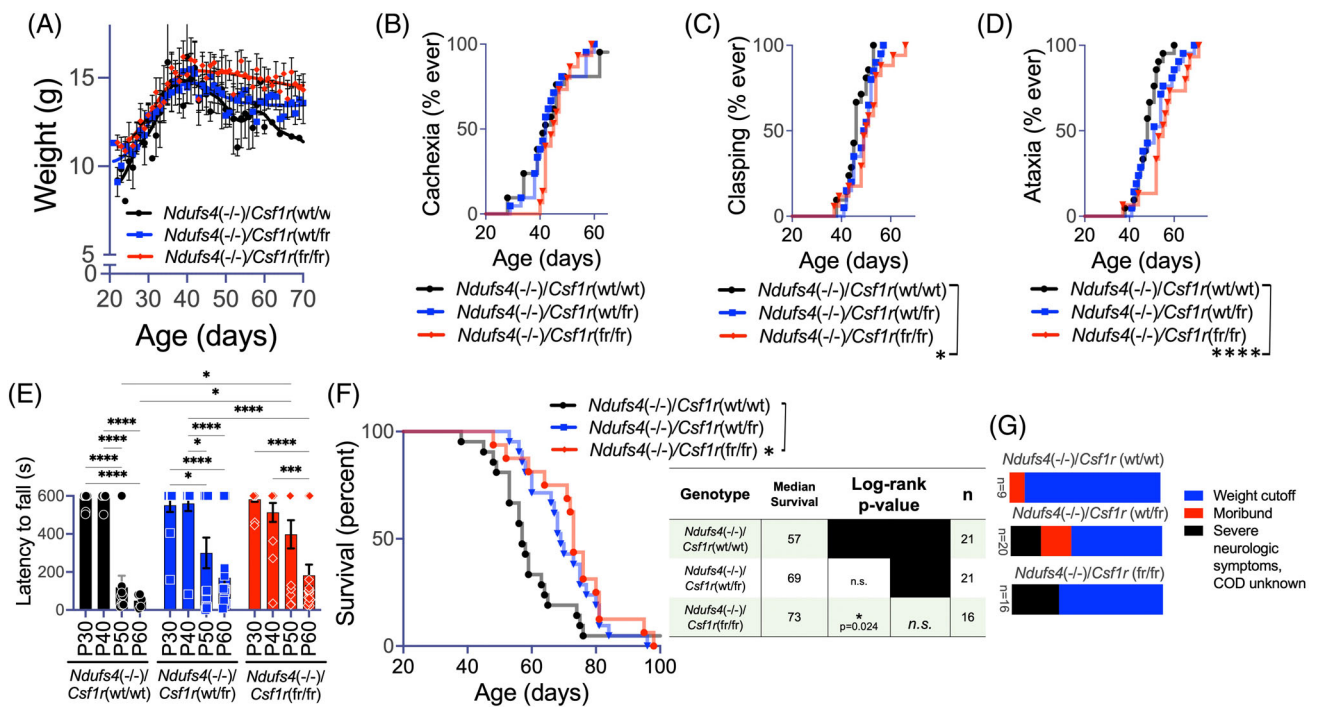


FIGURE 4 Genetic depletion of microglia provides limited benefits in the *Ndufs4(-/-)* model of LS. (A) Average weights of *Ndufs4(-/-)/Csf1r(wt/wt)*, *Ndufs4(-/-)/Csf1r(wt/fr)*, and *Ndufs4(-/-)/Csf1r(fr/fr)* mice. Disease onset, including onset of weight loss, occurs around the age of P37 in the *Ndufs4(-/-)* model of LS. Data shown are population averages with standard error of the mean (SEM) and Locally Weighted Scatterplot Smoothing (LOWESS) curves to reveal overall trends. (B) Onset of cachexia, defined as the date when progressive weight loss began, in *Ndufs4(-/-)/Csf1r(wt/wt)*, *Ndufs4(-/-)/Csf1r(wt/fr)*, and *Ndufs4(-/-)/Csf1r(fr/fr)* mice. * $p < 0.05$ by log-rank test. (C) Onset of forelimb clasping in *Ndufs4(-/-)/Csf1r(wt/wt)*, *Ndufs4(-/-)/Csf1r(wt/fr)*, and *Ndufs4(-/-)/Csf1r(fr/fr)* mice. * $p < 0.05$ by log-rank test. (D) Onset of ataxia in *Ndufs4(-/-)/Csf1r(wt/wt)*, *Ndufs4(-/-)/Csf1r(wt/fr)*, and *Ndufs4(-/-)/Csf1r(fr/fr)* mice. ** $p < 0.005$ by log-rank test. (E) Rotarod performance, as assessed by latency to fall (see Section 4), in *Ndufs4(-/-)/Csf1r(wt/wt)*, *Ndufs4(-/-)/Csf1r(wt/fr)*, and *Ndufs4(-/-)/Csf1r(fr/fr)* mice as a function of age. Two-way ANOVA row factor (age) **** $p < 0.0001$, column factor (genotype) * $p < 0.05$. * $p < 0.05$, ** $p < 0.005$, **** $p < 0.00005$ by Tukey's multiple comparisons corrected t -test, all rows and columns compared. (F) Survival of *Ndufs4(-/-)/Csf1r(wt/wt)*, *Ndufs4(-/-)/Csf1r(wt/fr)*, and *Ndufs4(-/-)/Csf1r(fr/fr)* mice. Median survival and statistical significance, by log-rank test, as shown. (G) Cause of death in *Ndufs4(-/-)/Csf1r(wt/wt)*, *Ndufs4(-/-)/Csf1r(wt/fr)*, and *Ndufs4(-/-)/Csf1r(fr/fr)* animals. See Figure S22 for respiratory function data.

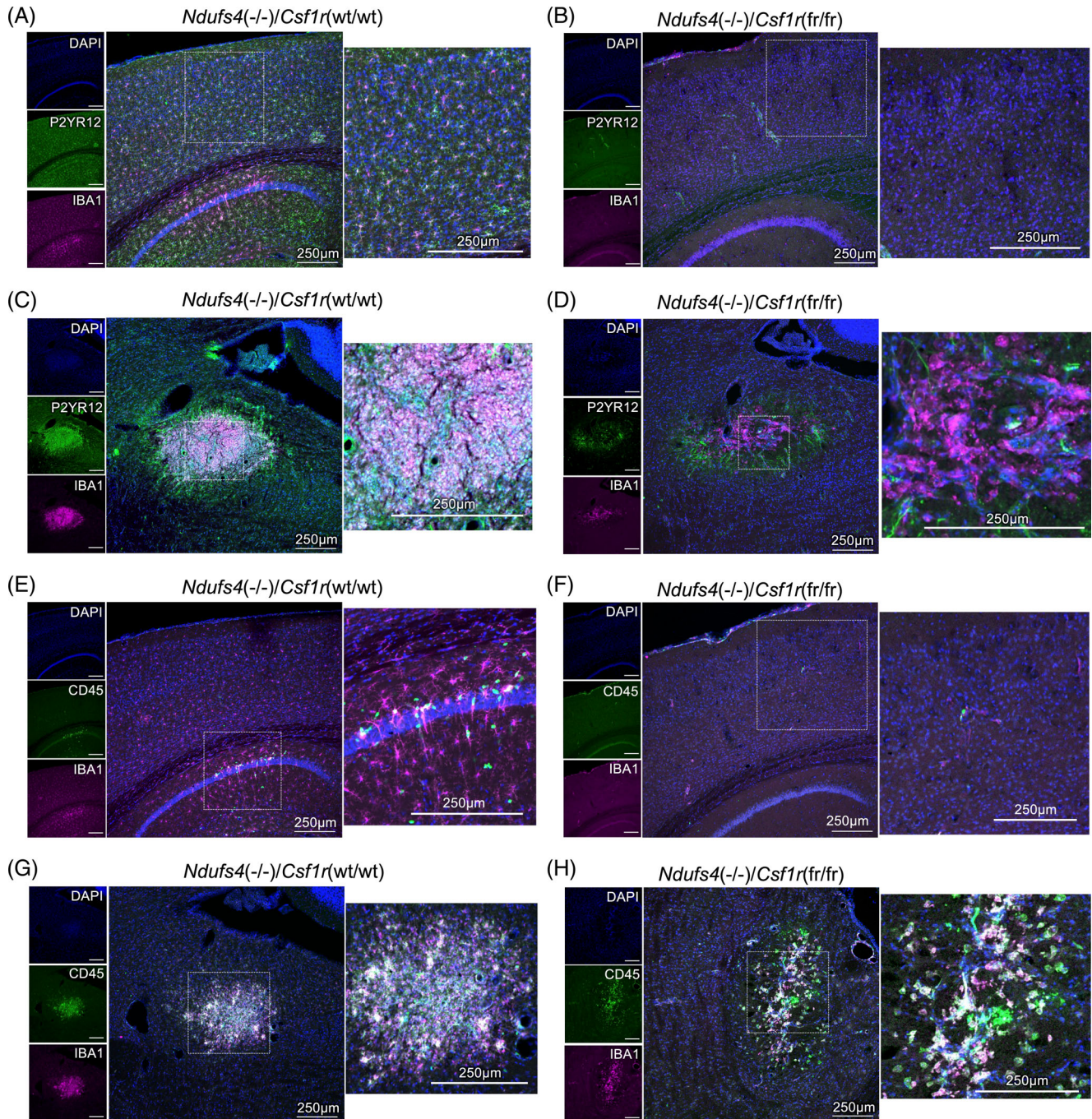


FIGURE 5 Peripheral macrophages in the CNS lesions characteristic of Leigh syndrome. For all panels, orientation is as in Figures 1–3 for the same brain regions. (A,B) Cortex of *Ndufs4(-/-)/Csf1r(wt/wt)* (A) and *Ndufs4(-/-)/Csf1r(fr/fr)* (B) mice stained for the pan-macrophage marker IBA1 (red) and the microglia-specific marker P2YR12 (green); DNA is co-stained with DAPI (blue). Microglia are absent by both IBA1 and P2YR12 staining in the *Ndufs4(-/-)/Csf1r(fr/fr)* cortex. (C,D) Brainstem lesions from *Ndufs4(-/-)/Csf1r(wt/wt)* (C) and *Ndufs4(-/-)/Csf1r(fr/fr)* (D) mice stained for the pan-macrophage marker IBA1 and the microglia-specific marker P2YR12. Cells positive for IBA1, the pan-macrophage marker, are present in both genotypes, while P2YR12 staining is absent in cells in the brainstem lesions of *Ndufs4(-/-)/Csf1r(fr/fr)* animals. The P2YR12 staining surrounding the lesion site does not appear to be cellular in origin, and is thought to reflect the presence of aggregated platelets, which are P2YR12 positive. (E,F) Cortex of *Ndufs4(-/-)/Csf1r(wt/wt)* (E) and *Ndufs4(-/-)/Csf1r(fr/fr)* (F) mice stained for the pan-macrophage marker IBA1 (red) and the peripheral leukocyte marker CD45 (green); DNA is co-stained with DAPI (blue). Microglia are absent in the *Ndufs4(-/-)/Csf1r(fr/fr)* cortex, and microglia (by IBA1 positivity and morphology) do not express CD45 (E). A few compact cells with CD45 positivity are present in both genotypes, presumed to be circulating leukocytes. (G,H) Brainstem lesions in *Ndufs4(-/-)/Csf1r(wt/wt)* (G) and *Ndufs4(-/-)/Csf1r(fr/fr)* (H) mice stained for the pan-macrophage marker IBA1 and the peripheral leukocyte marker CD45. CD45 positive cells are present in both in the *Ndufs4(-/-)/Csf1r(fr/fr)* and *Ndufs4(-/-)/Csf1r(wt/wt)* lesions, while most or all IBA1 positive cells in the *Ndufs4(-/-)/Csf1r(fr/fr)* lesion appear to be positive for the peripheral leukocyte marker CD45. Co-staining of CD45 and IBA1 is indicative of peripheral macrophages. Tissues collected from animals aged P55–66 in *Ndufs4(-/-)/Csf1r(wt/wt)*, and P75–80 in *Ndufs4(-/-)/Csf1r(fr/fr)*. Specific ages of tissue collection were determined by according to euthanasia criteria (i.e., animals were synchronized by relative disease stage), see Section 4. See Figures S23–S30 for enlargements of panels in Figure 1.

(Figure 5E,F). In brainstem lesions, *Ndufs4(-/-)/Csf1r* (wt/wt) mice both show strong staining for CD45 even when microglia are present, as determined by the presence of IBA1(+)/CD45(-) cells (Figure 5G). In *Ndufs4(-/-)/Csf1r(fr/fr)* animals, the cellularity of lesions appears reduced as was noted above (determined by overall DAPI nuclei numbers and density), and all or nearly all IBA(+) cells present appear to all be positive for CD45.

Together, these data indicate that peripheral macrophages contribute significantly to the cellular composition of CNS lesions in the *Ndufs4(-/-)* mouse model of LS, and that the absence of microglia reduces cellularity but has only modest effects on disease course.

3 | DISCUSSION

Here, we report that genetic depletion of microglia only modestly delays disease onset and progression in the *Ndufs4(-/-)* model of LS, contrasting with the previously reported rescue of disease resulting from high-dose pexidartinib treatment. Genetic depletion of microglia fails to prevent neuroinflammatory CNS lesion formation, the hallmark feature of LS, and associated sequelae of disease. Furthermore, CNS lesions in both *Ndufs4(-/-)/Csf1r(fr/fr)* animals include IBA(+)/CD45(+) cells, consistent with our prior findings that CNS lesions contain TMEM119(-)/IBA1(+) cells. Finally, while microglia appear to account for the majority of lesion cellularity in *Ndufs4(-/-)/Csf1r(wt/wt)* animals, lesion formation is not prevented in the absence of microglia and *Ndufs4(-/-)/Csf1r(fr/fr)* lesions are characterized by IBA(+)/P2YR12(-) peripheral macrophages. Together, these data demonstrate that peripheral macrophages play a prominent role in the pathogenesis of LS, including in CNS disease, and that the absence of microglia does not substantially alter disease course when circulating macrophages are intact.

The findings in this study are consistent with recent work by the Hidalgo laboratory, and our own prior work, demonstrating that low dose pexidartinib, used to eliminate microglia while sparing peripheral macrophages, only modestly alters disease course in the *Ndufs4(-/-)* [6, 18]. These data indicate that microglia contribute only partially to the pathogenesis of LS and that targeting microglia alone is insufficient to disrupt disease.

While depletion of microglia is not *sufficient* to prevent disease in the LS model, it remains to be determined whether microglia targeting is *necessary* to disrupt disease progression in the context of pharmacologic targeting of the immune system. In our histologic analysis of *Ndufs4(-/-)* mice with intact microglia, we see evidence for both microglia and peripheral macrophages in overt lesions. It seems likely that both microglia and macrophages causally contribute. The necessity and sufficiency of targeting peripheral macrophages must be assessed in

future studies, perhaps through antibody-mediated depletion of circulating macrophages. It is possible that some other pexidartinib responsive cell population mediates the benefits of that compound. Positive identification of the key causal cell types will require significant future work.

It is notable that the *Csf1r*ΔFIRE allele, even in the heterozygous state, provided a modest benefit to disease given that the number of microglia is not measurably reduced in these animals (Figure 1). This finding is consistent with the modest benefits of low dose pexidartinib treatment. While we find that low-dose pexidartinib is not effective in robustly altering disease course in the *Ndufs4(-/-)*, these observations suggest that low-dose CSF1R inhibitors may provide benefits in forms of mitochondrial disease, which involve CSF1R-dependent cells but are less severe, or progress less rapidly. For example, low-dose pexidartinib may attenuate disease in mitochondrial cerebellar ataxia caused by *Aifm1* deficiency, where microglial activation occurs in the absence of overt CNS lesions [19, 20]. It may be that differential activation of peripheral versus CNS immunity contributes to the distinct clinical presentations of unique forms of genetic mitochondrial disease, the mechanistic underpinnings of which have so far been elusive.

Given that there was no visible difference in the presentation of neurologic symptoms in the *Ndufs4(-/-)/Csf1r(fr/fr)* animals compared to *Ndufs4(-/-)* mice with intact microglia, we were surprised to find a general lack of IBA1(+) cells or signs of lesions in the cerebellum of *Ndufs4(-/-)/Csf1r(fr/fr)* mice. This finding suggests microglia are the dominant macrophage population driving cerebellar involvement, but that cerebellar involvement is not a major contributor to the overall *Ndufs4(-/-)* phenotype. It may be that microglia depletion would provide a significant benefit in forms of mitochondrial disease where cerebellar involvement is a prominent feature and survival is not limited by brainstem lesions, such as *Aifm1* related mitochondrial cerebellar ataxia.

It is also possible that our findings may be relevant to other human diseases which phenotypically mimic the symmetric neuroinflammatory CNS lesions seen in LS. These include progressive supranuclear palsy (PSP) and Wernicke's encephalopathy, diseases associated with exposure to environmental toxins that inhibit the mitochondrial ETC and thiamine deficiency, respectively; microglia activation appears to be a prominent factor in both cases [8, 21]. CSF1R targeting has recently been shown to benefit multiple complex neurodegenerative disease models including Parkinson's, multiple sclerosis, and Alzheimer's [22–25]. These findings suggest that the pathways we are probing here may be common to a range of diseases where evidence suggests causal roles for both immune activity and mitochondrial dysfunction. Future studies will be required to probe links to our findings in the setting of genetic mitochondrial dysfunction and

other forms of neurodegeneration, including age-related neurodegenerative diseases.

The relative failure of selective genetic or pharmacologic depletion of microglia to prevent disease, compared to pan-macrophage depletion with high-dose pexidartinib (see [6]), demonstrates a causal role for peripheral macrophages in the pathogenesis of Leigh syndrome. This is further supported by our findings that peripheral macrophages are present in the lesions of *Ndufs4(-/-)* animals whether microglia are present or not. While these data reveal a causal role for peripheral macrophages in the pathogenesis of Leigh syndrome, further studies will be needed to define early events in CNS neuroinflammation. We find that early post-disease onset brains show an enrichment of peripheral macrophages in at least one impacted brain region, the olfactory bulb (Figure S31), but have not found evidence for peripheral macrophages in brainstem in the absence of overt brainstem lesions. While genetic and pharmacologic depletion have established their causal role, future studies using macrophage targeted GFP and light-sheet or two-photon microscopy may allow for higher resolution description of the involvement of peripheral macrophages and microglia early in disease.

Many questions remain to be answered. For example, the nature of the inciting immune activating signal remains unknown. Nevertheless, we believe that there is a high potential for clinical translatability of recent work in this field. Supporting this notion, various case reports have indicated that immune modulatory therapies have altered disease course in LS and other genetic mitochondrial diseases [26–29] (evidence linking immune function to the pathogenesis of mitochondrial disease is summarized here [27]). The data presented here have important implications for any future efforts to translate immune-targeting strategies into treatments for genetic mitochondrial disease.

4 | METHODS

4.1 | Animals

Csf1r^{ΔFIRE/ΔFIRE} (which here we annotate as *Csf1r* (fr/fr)) mice are described in Rojo et al. [14] and were generously provided by the Jones laboratory at UC Irvine, originally provided to them by Dr Pridans at the University of Edinburgh. *Ndufs4*(+/-) mice were originally obtained from the Palmiter Laboratory at University of Washington, Seattle, WA, but are also available from the Jackson Laboratory (strain, 027058). Strain details are described in Kruse et al. [4]. Both the *Ndufs4* and *Csf1r*(fr/fr) lines are on the C57/BL6 background. *Ndufs4*(-/-) mice cannot be used for breeding due to their short lifespan and severe overt disease. *Ndufs4* (+/-) mice were bred with *Csf1r*(fr/fr) mice to produce double heterozygous offspring, which were then crossed to

produce *Ndufs4*(-/-)/*Csf1r*(wt/fr) and *Ndufs4*(-/-)/*Csf1r* (fr/fr) animals. *Csf1r*^{ΔFIRE} genotyping by polymerase chain reaction was performed using methods described in Rojo et al. [14]; genotyping of the *Ndufs4* allele was performed as in by Jackson Laboratory methods (strain 027058).

Mice were weaned at P20–22 days of age. *Ndufs4* (-/-) animals were housed with control littermates for warmth as *Ndufs4*(-/-) mice have low body temperature [4]. Mice were weighed and health assessed a minimum of three times a week. Wet food was provided in the bottom of the cage to *Ndufs4*(-/-) mice following symptom onset. Animals were euthanized if they reached a 20% loss of maximum body weight (measured 2 days consecutively), were immobile, or found moribund. Mice heterozygous for *Ndufs4* have no reported phenotype, so controls consisted of both heterozygous and wild-type *Ndufs4* animals. The *Ndufs4*(Ctrl) and *Ndufs4*(-/-) mice wild-type for FIRE (*Csf1r*(wt/wt)) used in this study came from crosses of *Ndufs4*(+/-)/*Csf1r*(fr/wt) mice and our general *Ndufs4* colony. Mice were fed PicoLab Diet 5058 and were on a 12-h light–dark cycle. All animal experiments followed Seattle Children’s Research Institute (SCRI) guidelines and were approved by the SCRI IACUC.

Clasping, circling, and ataxia were assessed by visual scoring and analyzed as previously described [30]. During disease progression *Ndufs4*(-/-) animals can display intermittent/transient improvement of symptoms. Here, we report whether the animal *ever* displayed the symptoms for two or more consecutive days.

The rotarod performance test was performed using a Med Associates ENV-571M single-lane rotarod. A mouse was placed on the rod already rotating at 6 rpm and latency to fall was timed for a maximum of 600 s while rotation remained constant. For each mouse, three trials were performed with a minimum of 10 min between each trial. The best of three trials was reported.

4.2 | Respiratory function

Breathing parameters were recorded from alert, unrestrained, ~P60 (±2 days) mice using whole-body plethysmography. Paired 300 mL recording and reference chambers were continuously ventilated (150 mL/min) normal air (79% N₂/21% O₂). Pressure differences between the recording and reference chambers were measured (Buxco) and digitized (Axon Instruments) to visualize respiratory pattern. Mice were allowed to acclimate to the chambers for 30–40 min prior to acquisition of 35 min of respiratory activity in normal air. Respiratory frequency and breath-to-breath irregularity scores ($irreg.score = ABS\left(\frac{N-(N-1)}{N}\right)$) of frequency and amplitude (peak inspiratory airflow) were quantified during periods of resting breathing (pClamp10 software).

4.3 | Brain collection, immune-staining, and imaging

Tissue was collected for *Ndufs4*(Ctrl) mice between P60 and P66 and for *Ndufs4*($-/-$) mice when euthanasia criteria were met. Mice were fixed-perfused with 20 mL of PBS followed by 20 mL of pre-chilled (4°C) 4% PFA. Immediately following perfusion, the brain was removed and placed in 4% PFA for a minimum of 24 h at 4°C. The brain was then moved to cryoprotection solution (30% sucrose, 1% DMSO, 100 μ M glycine, 1 \times PBS) for a minimum of 48 h at 4°C. Cryopreserved tissue was frozen in cryomedia in cryoblocks on dry ice and stored at -80°C until cryosectioning. Cryoblocks were sectioned at 50 μ m thickness using a Leica CM3050S Cyrostat set at -20°C . Slices were immediately placed in 1 \times PBS with 1 μ g/mL DAPI at 4°C for a maximum of 24 h before mounting on slides. Prior to mounting, slices were examined for the presence lesions using a fluorescent microscope. Slices with lesions were mounted on Superfrost plus slides. Four to five slices were mounted on each slide. For control animals, similar anatomic sections were chosen for mounting. Sections from the center of the lesion were chosen for staining and are shown here.

Mounted sections were baked at 37°C in a white-light LED illuminated incubator for 24 h before storing at -80°C until staining. For immunofluorescent staining, slides were incubated for 24 h at 60°C in pH 6.0 citrate antigen retrieval buffer. Following antigen retrieval, slides were washed for 5 min in 1 \times PBS on ice before being incubated for 1 h on ice in 1 mg/mL sodium borohydride in PBS. Slides were then washed in 1 \times PBS with 10 mM glycine for 5 min before being placed in a 0.5 mg/mL Sudan Black in 70% ethanol and incubated overnight with gentle stirring. Slides were then washed for 5 min 3 \times in 1 \times PBS. Excess moisture was wiped away and a hybriwell sealing sticker (Grace Bio-Labs, GBL612202) applied to each slide over the tissue slices. Slides were incubated for 30 min at room temperature in blocking/permeabilization solution (1 mM digitonin, 10% rabbit serum, 0.5% tween in 1 \times PBS). Following blocking, the hybriwell sealing stickers were removed and blocking solution shaken off the slides. Excess moisture was wiped away and new hybriwells were placed. The slides were incubated for 24 h at 4°C in antibodies and 1 μ g/mL DAPI diluted in the blocking solution. The following fluorescently conjugated primary antibodies were used: Anti-IBA1 (1:150, Wako 013-26471), anti-GFAP (1:300, clone GA5, Invitrogen 14-9892-82). After incubation, slides were washed 4 \times 5 min in 1 \times PBS. ProLong Gold Antifade was used as mounting media and coverslips sealed with clear nail polish. Slides were stored in an opaque slide box at 4°C. The following unconjugated primary antibody was used: P2RY12 (1:100), clone S16D007D, Biolegend, 848002. Unconjugated primary and conjugated primary were both included in the initial 24-h incubation, followed by 4 \times 5 min washes in

1 \times PBS. Slides were then incubated in conjugated secondary antibody (1:500, anti-rat IgG AF-488 conjugate, Cell Signalling Technologies, #4416) and DAPI (1 μ g/mL) for 2 h at room temperature. Slides were then washed and cover slipped as described above.

Imaging was performed on a Zeiss LSM710 confocal microscope. Images were collected using a 10 \times objective with a 0.6 \times optical zoom. Channels were set to an optical thickness of 15 μ m or 25 nm. 15 μ m images were used for quantifying IBA1(+) cells; 25 μ m sections were imaged for Figures 3–5. DAPI was excited with a 405 nm laser, Alexa488 with a 488 nm laser, and fluorochrome 635 (IBA1, Wako) at 633 nm. Images were taken with the same laser intensity and collection filter settings. Gain/brightness/contrast were arbitrarily adjusted for visualization to make cell morphology clearly visible (intensities not compared).

IBA1(+) cells were counted using ImageJ. Brightness and contrast were adjusted in ImageJ to enhance visualization of cell morphology. Cells were counted based on IBA1 positivity, not intensity, so this does not impact the results. Image areas of roughly the same size and anatomical location were chosen and all cells in that region were counted and the number of cells per mm² calculated. Only one image from each mouse was counted.

4.4 | Statistical analysis

All statistical analyses were performed using GraphPad Prism. Error bars represent standard error of the mean (SEM) and $p < 0.05$ is considered statistically significant.

4.5 | Scientific rigor

Sex—approximately equal numbers of male and female animals were used in each experiment. No significant sex differences have been reported in *Ndufs4*($-/-$) or *Csf1r*(fr/fr) mice and none were observed here.

4.6 | Exclusion criteria

Animals euthanized prior to the age of disease onset in the *Ndufs4*($-/-$) were excluded from study. Our criteria for early life exclusion includes severe weaning stress (significant weight loss or spontaneous mortality before P30), runts (defined as ≤ 5 g body weight at weaning age), or those or born with health issues unrelated to the *Ndufs4*($-/-$) phenotype (such as hydrocephalus). These criteria are applied to all genotypes as part of our standard animal care.

AUTHOR CONTRIBUTIONS

Allison R. Hanaford, Nathan Andrew Baertsch, Vandana Kalia, and Surojit Sarkar: conception of work; design of

work, acquisition and analysis of data; interpretation of data; and manuscript drafting and revision. **Katerina James, Yihan Chen, Michael Mulholland, Vivian Truong, and Ryan W. Liao:** acquisition and analysis of data. **Bernhard Kayser and Asheema Khanna:** acquisition and analysis of data; interpretation of data. **Phil Morgan and Margaret Sedensky:** interpretation of data; and manuscript drafting and revision. **Simon C. Johnson:** conception of work; design of work; acquisition and analysis of data; interpretation of data; and manuscript drafting and revision.

ACKNOWLEDGMENTS

The authors have nothing to report.

FUNDING INFORMATION

National Institutes of Health grant NIH/NINDS R01NS119426 (Simon C. Johnson). National Institutes of Health grant NIH/GM R01-133865 (Margaret Sedensky and Simon C. Johnson). Northwest Mitochondrial Research Guild (Simon C. Johnson, Allison R. Hanaford, Bernhard Kayser). No funder had any direct role in design of the study, collection, analysis, and interpretation of data, or writing of the manuscript.

CONFLICT OF INTEREST STATEMENT

The authors declare no conflicts of interest.

DATA AVAILABILITY STATEMENT

All data generated or analyzed during this study are included in this published article and its supplementary information files, with the exception of raw image files. These are available from the corresponding author on reasonable request.

ETHICS STATEMENT

All animal experiments were performed at Seattle Children's Research Institute (SCRI), followed SCRI guidelines, and were approved by the SCRI institutional animal care and use committee (IACUC).

ORCID

Simon C. Johnson  <https://orcid.org/0000-0002-1942-3674>

REFERENCES

- Lake NJ, Bird MJ, Isohanni P, Paetau A. Leigh syndrome: neuropathology and pathogenesis. *J Neuropathol Exp Neurol.* 2015;74:482–92. <https://doi.org/10.1097/NEN.0000000000000195>
- Lake NJ, Compton AG, Rahman S, Thorburn DR. Leigh syndrome: one disorder, more than 75 monogenic causes. *Ann Neurol.* 2016;79:190–203. <https://doi.org/10.1002/ana.24551>
- Hong CM, Na JH, Park S, Lee YM. Clinical characteristics of early-onset and late-onset Leigh syndrome. *Front Neurol.* 2020;11:267. <https://doi.org/10.3389/fneur.2020.00267>
- Kruse SE, Watt WC, Marcinek DJ, Kapur RP, Schenkman KA, Palmiter RD. Mice with mitochondrial complex I deficiency develop a fatal encephalomyopathy. *Cell Metab.* 2008;7:312–20. <https://doi.org/10.1016/j.cmet.2008.02.004>
- van de Wal MAE, Adjubo-Hermans MJW, Keijer J, Schirris TJJ, Homberg JR, Wieckowski MR, et al. Ndufs4 knockout mouse models of Leigh syndrome: pathophysiology and intervention. *Brain.* 2022;145:45–63. <https://doi.org/10.1093/brain/awab426>
- Stokes JC, Bornstein RL, James K, Park KY, Spencer KA, Vo K, et al. Leukocytes mediate disease pathogenesis in the Ndufs4 (KO) mouse model of Leigh syndrome. *JCI Insight.* 2022;7:e156522. <https://doi.org/10.1172/jci.insight.156522>
- Stanley ER, Chitu V. CSF-1 receptor signaling in myeloid cells. *Cold Spring Harb Perspect Biol.* 2014;6:a021857. <https://doi.org/10.1101/cshperspect.a021857>
- Alster P, Madetko N, Koziorowski D, Friedman A. Microglial activation and inflammation as a factor in the pathogenesis of progressive supranuclear palsy (PSP). *Front Neurosci.* 2020;14:893. <https://doi.org/10.3389/fnins.2020.00893>
- Liu Y, Given KS, Dickson EL, Owens GP, Macklin WB, Bennett JL. Concentration-dependent effects of CSF1R inhibitors on oligodendrocyte progenitor cells ex vivo and in vivo. *Exp Neurol.* 2019;318:32–41. <https://doi.org/10.1016/j.expneurol.2019.04.011>
- Leigh D. Subacute necrotizing encephalomyelopathy in an infant. *J Neurol Neurosurg Psychiatry.* 1951;14:216–21. <https://doi.org/10.1136/jnnp.14.3.216>
- Quintana A, Kruse SE, Kapur RP, Sanz E, Palmiter RD. Complex I deficiency due to loss of Ndufs4 in the brain results in progressive encephalopathy resembling Leigh syndrome. *Proc Natl Acad Sci U S A.* 2010;107:10996–1001. <https://doi.org/10.1073/pnas.1006214107>
- Ito D, Imai Y, Ohsawa K, Nakajima K, Fukuuchi Y, Kohsaka S. Microglia-specific localisation of a novel calcium binding protein, Iba1. *Brain Res Mol Brain Res.* 1998;57:1–9. [https://doi.org/10.1016/s0169-328x\(98\)00040-0](https://doi.org/10.1016/s0169-328x(98)00040-0)
- Ye F, Yang J, Hua Y, Keep RF, Xi G. Novel approach to visualize microglia death and proliferation after intracerebral hemorrhage in mice. *Stroke.* 2022;53:e472–6. <https://doi.org/10.1161/STROKEAHA.122.040302>
- Rojo R, Raper A, Ozdemir DD, Lefevre L, Grabert K, Wollscheid-Lengeling E, et al. Deletion of a Csf1r enhancer selectively impacts CSF1R expression and development of tissue macrophage populations. *Nat Commun.* 2019;10:3215. <https://doi.org/10.1038/s41467-019-11053-8>
- Himes SR, Tagoh H, Goonetilleke N, Sasmono T, Oceandy D, Clark R, et al. A highly conserved c-fms gene intronic element controls macrophage-specific and regulated expression. *J Leukoc Biol.* 2001;70:812–20.
- Erblich B, Zhu L, Etgen AM, Dobrenis K, Pollard JW. Absence of colony stimulation factor-1 receptor results in loss of microglia, disrupted brain development and olfactory deficits. *PLoS One.* 2011;6:e26317. <https://doi.org/10.1371/journal.pone.0026317>
- Rojo R. Role of the fms-intronic regulatory element (FIRE) in macrophage development. *Developmental Biology, University of Edinburgh.* 2018.
- Aguilar K, Comes G, Canal C, Quintana A, Sanz E, Hidalgo J. Microglial response promotes neurodegeneration in the Ndufs4 KO mouse model of Leigh syndrome. *Glia.* 2022;70:2032–44. <https://doi.org/10.1002/glia.24234>
- Klein JA, Longo-Guess CM, Rossmann MP, Seburn KL, Hurd RE, Frankel WN, et al. The harlequin mouse mutation downregulates apoptosis-inducing factor. *Nature.* 2002;419:367–74. <https://doi.org/10.1038/nature01034>
- Wischof L, Gioran A, Sonntag-Bensch D, Piazzesi A, Stork M, Nicotera P, et al. A disease-associated Aifm1 variant induces severe myopathy in knockin mice. *Mol Metab.* 2018;13:10–23. <https://doi.org/10.1016/j.molmet.2018.05.002>
- Wang D, Hazell AS. Microglial activation is a major contributor to neurologic dysfunction in thiamine deficiency. *Biochem Biophys Res Commun.* 2010;402:123–8. <https://doi.org/10.1016/j.bbrc.2010.09.128>



22. Groh J, Klein D, Berve K, West BL, Martini R. Targeting microglia attenuates neuroinflammation-related neural damage in mice carrying human PLP1 mutations. *Glia*. 2019;67:277–90. <https://doi.org/10.1002/glia.23539>
23. Marzan DE, Brugger-Verdon V, West BL, Liddelow S, Samanta J, Salzer JL. Activated microglia drive demyelination via CSF1R signaling. *Glia*. 2021;69:1583–604. <https://doi.org/10.1002/glia.23980>
24. Sosna J, Philipp S, Albay R 3rd, Reyes-Ruiz JM, Baglietto-Vargas D, LaFerla FM, et al. Early long-term administration of the CSF1R inhibitor PLX3397 ablates microglia and reduces accumulation of intraneuronal amyloid, neuritic plaque deposition and pre-fibrillar oligomers in 5XFAD mouse model of Alzheimer's disease. *Mol Neurodegener*. 2018;13:11. <https://doi.org/10.1186/s13024-018-0244-x>
25. Yang X, Ren H, Wood K, Li M, Qiu S, Shi FD, et al. Depletion of microglia augments the dopaminergic neurotoxicity of MPTP. *FASEB J*. 2018;32:3336–45. <https://doi.org/10.1096/fj.201700833RR>
26. Edmonds JL, Kirse DJ, Kearns D, Deutsch R, Spruijt L, Naviaux RK. The otolaryngological manifestations of mitochondrial disease and the risk of neurodegeneration with infection. *Arch Otolaryngol Head Neck Surg*. 2002;128:355–62. <https://doi.org/10.1001/archotol.128.4.355>
27. Hanaford A, Johnson SC. The immune system as a driver of mitochondrial disease pathogenesis: a review of evidence. *Orphanet J Rare Dis*. 2022;17:335. <https://doi.org/10.1186/s13023-022-02495-3>
28. Lee YJ, Hwang SK, Kwon S. Acute necrotizing encephalopathy in children: a long way to go. *J Korean Med Sci*. 2019;34:e143. <https://doi.org/10.3346/jkms.2019.34.e143>
29. Walker MA, Slate N, Alejos A, Volpi S, Iyengar RS, Sweetser D, et al. Predisposition to infection and SIRS in mitochondrial disorders: 8 years' experience in an academic center. *J Allergy Clin Immunol Pract*. 2014;2:465–8, 468.e1. <https://doi.org/10.1016/j.jaip.2014.02.009>
30. Johnson SC, Yanos ME, Kayser EB, Quintana A, Sangesland M, Castanza A, et al. mTOR inhibition alleviates mitochondrial disease in a mouse model of Leigh syndrome. *Science*. 2013;342:1524–8. <https://doi.org/10.1126/science.1244360>

SUPPORTING INFORMATION

Additional supporting information can be found online in the Supporting Information section at the end of this article.

How to cite this article: Hanaford AR, Khanna A, Truong V, James K, Chen Y, Mulholland M, et al. Peripheral macrophages drive CNS disease in the *Ndufs4*(*-/-*) model of Leigh syndrome. *Brain Pathology*. 2023;33(6):e13192. <https://doi.org/10.1111/bpa.13192>